Skull Base Tumor Mimics

Jeffrey H. Huang, MD[a], Mari Hagiwara, MD[b,*]

KEYWORDS

• Skull base • Petrous apex • Mimics

KEY POINTS

- The ability to confidently identify anatomic variants and benign pathologies that can mimic neoplasm in the skull base may help prevent unnecessary imaging follow-up, biopsies, or interventions.
- Normal variant anatomy of the central skull base includes canalis basilaris medianus, fossa navicularis magna, craniopharyngeal canal, and arrested pneumatization of the sphenoid sinus.
- Benign lesions of the central skull base include cephalocele, fibrous dysplasia, ecchordosis physaliphora, invasive or ectopic pituitary adenoma, skull base osteomyelitis, and other inflammatory processes.
- Petrous apex tumor mimics include petrous apex cephalocele, asymmetric pneumatization, petrous apex effusion, and petrous internal carotid artery aneurysm.

INTRODUCTION

The base of skull acts as a supporting structure for the brain and the primary boundary between the intracranial central nervous system and the extracranial head and neck compartments. Many different benign and malignant processes can affect the skull base, and its involvement by malignant processes can drastically alter staging, surgical approach, or radiation planning.[1–4] Clinical evaluation and tissue sampling are difficult because of its deep location, leaving imaging assessment the primary means for lesion evaluation. The purpose of this article is to familiarize readers with the imaging characteristics of various anatomic variants and benign pathologies of the skull base that can mimic more ominous pathologies, in hopes of increasing confidence of diagnosis, decreasing unnecessary procedures, and allaying patient fear.

ANATOMIC VARIANTS OF THE CENTRAL SKULL BASE

The embryologic development of the sphenoid bone is complex, with 15 separate ossification centers, containing the cephalic end of the course of the notochord, and also taking part in development of the pituitary gland.[5–8] Failure of embryologic development could produce anatomic variants including canalis basilaris medianus (CBM), fossa navicularis magna, and craniopharyngeal canal (CPC), which radiologists should be familiar with to avoid misinterpretation as pathology.

Canalis Basilaris Medianus

Anatomic variants of the basiocciput are uncommon, and the CBM, also known as the median clival canal, clival canal, or median basal canal, is one of the more well-known variants.[5,9] The CBM was first described by Gruber in 1880 and consists of a well-defined channel extending from the surface of the basiocciput.[5] Depending on the number and location of openings to the surface of the basiocciput, six different types have been described, and they are estimated to occur in about 4% to 5% of children and 2% to 3% of adults (**Fig. 1**).[5,6,9–14] These defects may close as children age, explaining the discrepancy between incidences in children and adults.

[a] Department of Radiology, NYU Langone Health, 462 1st Avenue, NBV-3W38, New York, NY 10016, USA; [b] Department of Radiology, NYU Langone Health, 222 East 41st Street, 5th Floor Radiology, New York, NY 10017, USA
* Corresponding author.
E-mail address: Mari.Hagiwara@nyulangone.org

Neuroimag Clin N Am 32 (2022) 327–344
https://doi.org/10.1016/j.nic.2022.02.001
1052-5149/22/

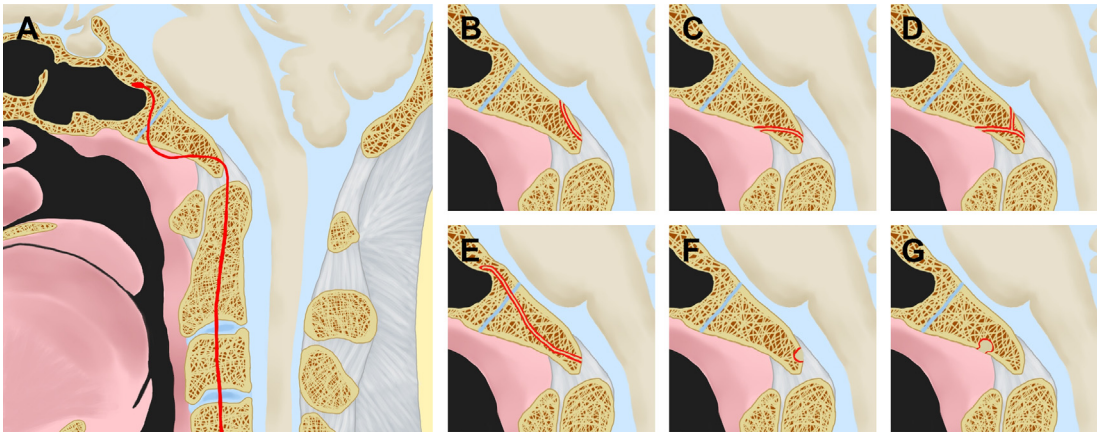

Fig. 1. Canalis basilaris medianus. The developmental notochord extends cranially to caudally through the sphenoid, sphenoccipital synchondrosis, occiput, vertebral bodies, and intervertebral disks, with a free segment in the nasopharynx (*A*). CBM complete types include superior (*B*), inferior (*C*), and bifurcatus (*D*). CBM incomplete types include long-channel (*E*), superior recess (*F*), and inferior recess (*G*).

Three types of complete CBM have been described. The superior type exhibits a superior-inferior channel through the clivus connecting two openings on the dorsal aspect of the basiocciput. The inferior type exhibits an anterior-posterior channel connecting openings on the dorsal and ventral aspects of the basiocciput. The bifurcatus type exhibits a bifurcated channel connecting two openings on the dorsal aspect and one opening on the ventral aspect of the basiocciput.

Three types of incomplete CBM have been described. The long-channel type exhibits a long channel extending from the dorsal aspect of the basiocciput toward the basisphenoid. The superior and inferior recess types exhibit round defects along the dorsal and ventral aspects of the basiocciput (see **Fig. 1**).

On imaging, the complete types or the incomplete long channel type appear as 1- to 2-mm wide, well-corticated, midline, channel-like defects extending from the dorsal aspect of the basiocciput (**Fig. 2**). The incomplete recess types appear as round, well-corticated midline defects along the surface of the basiocciput and may contain adenoid lymphoid tissue in the case of the inferior recess type, which is misinterpreted as a mass. The longitudinal extent of the CBM may be more easily assessed on thin-slice sagittal computed tomography (CT) images.

There are two main theories explaining the development of the CBM.[5,6,15] The first is that the CBM is simply a vascular channel containing venous structures (emissary veins) connecting to the basilar venous plexus. A few studies have demonstrated only the presence of vascular structures within the canal.[9,14] The second, more likely theory is that the CBM represents remnant notochordal tissue. In utero, the notochord courses within the vertebral bodies caudally. Cranially, the notochord courses within the basiocciput and ends in the posterior sphenoid, with a free segment within the pharyngeal wall ventral to the clivus.[5,6,15] The notochord is enclosed by the osseous structures and degenerates, leaving remnants within the clivus and nucleus pulposi.[6,15] Failure of different portions of the notochordal canal to close entirely is thought to result in the CBM.

Although the CBM is generally thought to be a benign anatomic variant, there have been case reports of potentially related complications. Nguyen and colleagues[16] reported a case of a nasopharyngeal chordoma associated with a CBM, which also lends credence to the theory that the CBM represents remnant notochordal tissue. Additional potential complications include basioccipital meningocele, recurrent meningitis, pharyngeal enterogenous cysts, nasopharyngeal Tornwaldt cysts, and cerebrospinal fluid (CSF) leaks.[6,17–22]

Fossa Navicularis Magna

The fossa navicularis magna, also known as the fossa pharyngea, large pharyngeal fossa, keyhole defect, CBM, and longitudinal or transverse segmentations, is another anatomic variant of the ventral aspect of the basiocciput.[5,23,24] It is estimated to occur in approximately 1% to 8% of the population, without any significant difference in incidence between males and females.[11,25–27]

On imaging, the fossa navicularis magna appears as a well-defined, well-corticated, notchlike midline defect along the ventral aspect of the clivus and contains soft tissue (**Fig. 3**), similar in

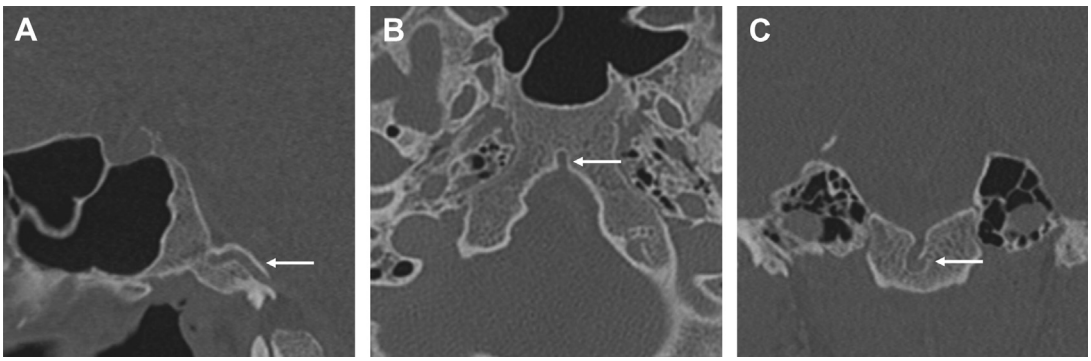

Fig. 2. Incomplete long channel type canalis basilaris medianus. Sagittal (*A*), axial (*B*), and coronal (*C*) computed tomography images demonstrate a long, thin, well-corticated, channel-like midline osseous defect in the dorsal surface of the clivus, extending from the dorsal aspect of the basiocciput toward the basisphenoid (*arrows*). (*Courtesy of* G. Moonis, MD, New York, New York).

appearance to the inferior recess type CBM.[5,23,24,28] It can appear as a keyhole-shaped defect, with a narrow neck extending to a deep larger round defect. It may contain lymphoid tissue from the nasopharyngeal adenoids.[24] At the bottom of the fossa navicularis, there may be a round or ovoid recess, called the pharyngeal fossa.[5,28]

Given the similarity of its appearance, the fossa navicularis magna may actually represent the inferior recess variant of an incomplete CBM.[5,23,28] It is also thought to represent remnant notochordal tissue, rather than prominent emissary veins.[5,29]

The fossa navicularis magna is generally thought to be a benign anatomic variant, but it may occasionally serve as a route of spread for infection via primary infection or abscess formation within the lymphoid tissue of the fossa navicularis, resulting in clival osteomyelitis and intracranial spread.[11,28–31]

Craniopharyngeal Canal

The CPC, also known as the persistent CPC, persistent hypophyseal canal, or transsphenoidal canal, is another skull base anatomic variant, appearing as a well-corticated, midline, linear defect of the sphenoid, extending from the floor of the sella turcica to the nasopharynx.[7,8,32,33] It is rare, occurring in approximately 0.3% to 0.4% of the population, and larger defects may actually reflect meningoencephaloceles related to dysraphism and occur with other midline craniofacial abnormalities, such as optic apparatus abnormalities, agenesis of the corpus callosum, PHACES syndrome, cleft lip, or cleft palate.[11,32–34]

The pituitary gland is formed by fusion of Rathke pouch, which forms as a diverticulum from the roof of the stomodeum migrating superiorly, with the floor of the diencephalon migrating inferiorly.[8] The presphenoid and postsphenoid cartilages then fuse, resulting in closure of Rathke pouch. Failure of the cartilage to fuse leaves behind a residual canal, the CPC.[7,8,32,33] Remnant pituitary tissue has been found within a CPC, supporting this theory.[35]

Although the CPC is a benign variant, its presence may have important clinical and surgical implications. A large CPC may be lined by dura that joins with the periosteum on the undersurface of the sphenoid, resulting in CSF leaks or recurrent

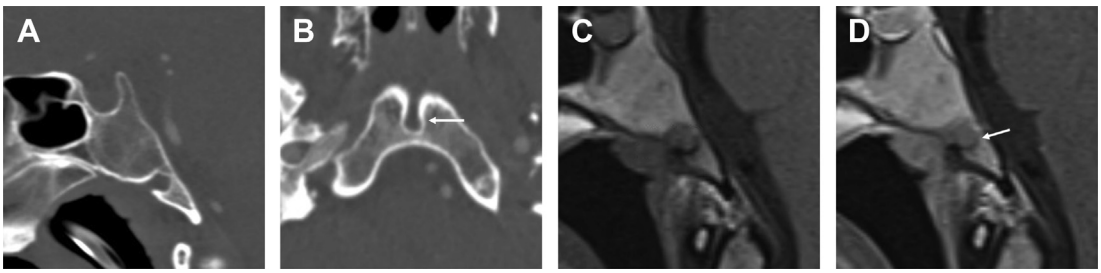

Fig. 3. Fossa navicularis. Sagittal CT image (*A*) shows a round, well-corticated osseous notchlike midline defect in the ventral surface of the clivus containing soft tissue. Axial CT image (*B*) shows the defect is midline, with a keyhole configuration (*arrow*). Noncontrast (*C*) and contrast-enhanced (*D*) T1-weighted (T1W) MR images show the soft tissue within the fossa is continuous with and enhances similarly to the nasopharyngeal tissues, reflecting adenoidal lymphoid tissue (*arrow*).

meningitis.[33,36–40] The pituitary gland itself may herniate through the canal and the canal may be associated with masses, such as pituitary adenomas, craniopharyngiomas, dermoids, and nasopharyngeal gliomas (heterotopic neuroglial tissue), which is mistaken for skull base or primary nasopharyngeal polyps or neoplasm. Pituitary tissue may be inadvertently resected during surgery, resulting in iatrogenic hypopituitarism or CSF leak.[7,8,32,41–44]

In 2014, Abele and colleagues[8] proposed a classification system composed of three main types of CPC. Type 1 is described as a small incidental canal (**Fig. 4**), type 2 as a medium-sized canal containing ectopic adenohypophysis, type 3A as a large canal with associated cephalocele, type 3B as a large canal with associated tumors of the adenohypophysis or associated embryonic tissues (**Fig. 5**), and type 3C as a large canal with associated tumors of both tissue types. Type 2 and type 3 CPC may be associated with higher rates of pituitary dysfunction, and type 3 CPC may be more prone to surgical complications, such as iatrogenic hypopituitarism or CSF leak.

Arrested Pneumatization of the Sphenoid Sinus

Pneumatization of the paranasal sinuses begins in utero, with maturation continuing through the third decade of life.[45–49] Alteration of this process can result in hypoplastic, aplastic, or accessory sinuses. Arrested pneumatization, most frequently involving the sphenoid sinus, is a developmental variant with imaging features that may be easily confused with more concerning pathologies.[45,50,51]

At birth, the sphenoid bones contain erythropoietic marrow, which undergoes yellow fatty marrow conversion within the presphenoid plate starting before 2 years of age.[45–48] The process extends posteriorly into the basisphenoid. Conversion here precedes the normal marrow conversion of the clivus.[45] Respiratory mucosa extends into the areas of yellow marrow and results in pneumatization as early as 2 years of age and extends to the sphenoccipital synchondrosis, attaining maturity by 14 to 16 years.[45–49] Marrow conversion is thought to be triggered by changes in blood supply or oxygenation, but it is not clearly understood.[48,52] Patients with sickle cell or thalassemia, with diseased red blood cells, seem to have higher rates of arrested pneumatization, lending credence to this idea.[51]

When arrested pneumatization occurs, atypical fatty marrow persists within the sphenoid bone adjacent to the aerated sinuses, most commonly in expected regions of normal or accessory sphenoid sinus pneumatization. These locations include the basisphenoid, pterygoid processes, and clivus.[45] On CT, it appears as a well-circumscribed, nonexpansile lesion with well-corticated margins and varying amounts of internal fat and internal curvilinear calcifications.[45] On MR imaging, it appears as a lesion with higher T1 signal than that of surrounding normal bone marrow (**Fig. 6**) and may have subtle patchy enhancement.[45] Given its imaging features, it may be misinterpreted as chordoma, chondrosarcoma, fibrous dysplasia (FD), osteomyelitis, or metastatic disease and can lead to unnecessary imaging, biopsy, or treatment.[45,50]

To allow for more confident diagnosis of arrested pneumatization, Welker and colleagues[45] in 2008 proposed a set of diagnostic criteria: (1) location at a site of normal or accessory pneumatization; (2) nonexpansile lesion with sclerotic, well-circumscribed margins; and (3) demonstrating fat content, internal curvilinear

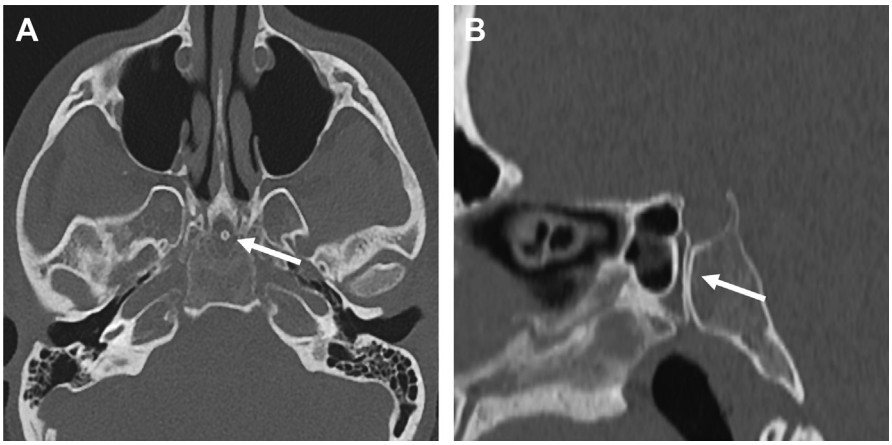

Fig. 4. Type 1 CPC. Axial (*A*) and sagittal (*B*) CT images show a narrow, well-corticated, midline channel through the clivus, extending from the floor of the sella turcica to the roof of the nasopharynx (*arrows*).

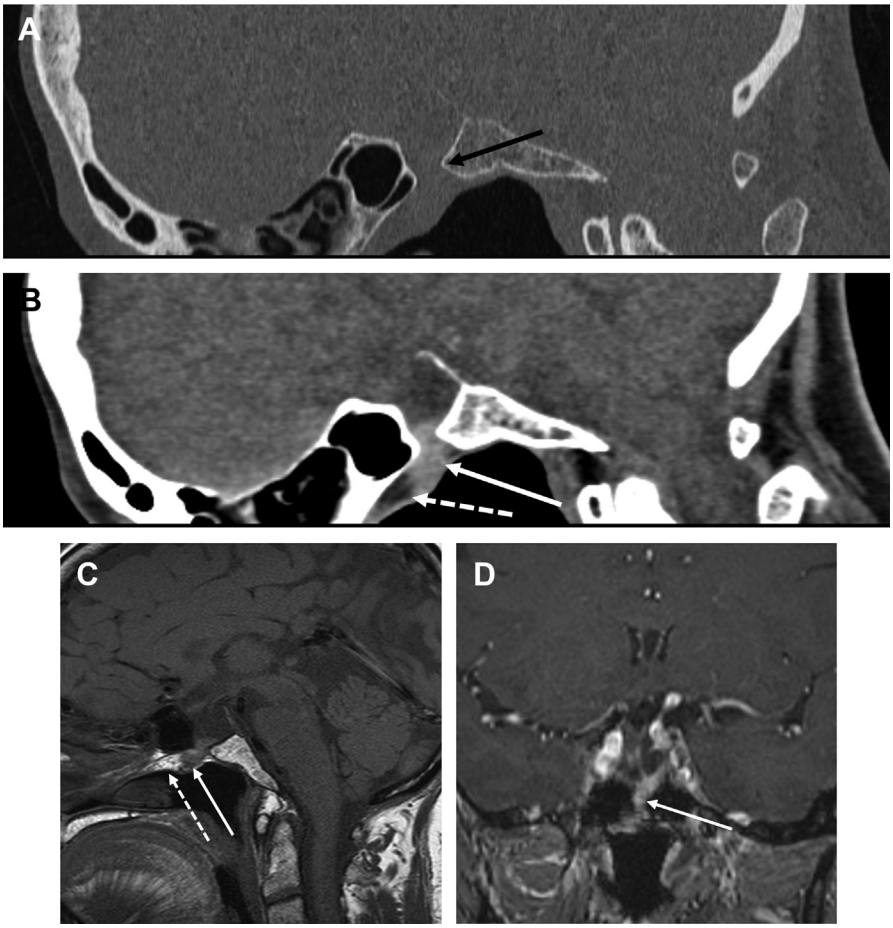

Fig. 5. Type 3B CPC. Sagittal CT images in bone (*A*) and soft tissue (*B*) windows show a large well-corticated craniopharyngeal canal/defect (*black arrow*) in the floor of the sella turcica, with herniated pituitary tissue (*white arrow*) and a fat-containing lesion anteriorly, likely a dermoid (*dashed arrow*). Sagittal precontrast (*C*) and coronal postcontrast (*D*) T1W MR images show the enhancing herniated pituitary tissue (*solid arrows*) and T1 hyperintense dermoid (*dashed arrow*).

calcifications, and normal appearance of any associated skull base foramina.

BENIGN LESIONS

Cephalocele

Cephaloceles are an extension or protrusion of any intracranial contents through a defect of the cranium and dura mater.[53–55] When they contain herniated brain tissue, they are termed encephaloceles. Congenital cephaloceles are rare, with an incidence of approximately 0.8 to 4 per 10,000 live births. They are thought to represent a primary anomaly of formation and separation of the neural tube from the body surface. As a result, they occur in conjunction with other intracranial and extracranial developmental anomalies in up to 50%.[53–60] These more commonly occur posteriorly (occipital or parietal) than anteriorly (frontoethmoidal),[54–56] and they are most often midline but can occur off midline, such as into the paranasal sinuses or petrous apices.[53,61,62]

Acquired cephaloceles can occur as a result of prior trauma, surgery, tumors, sphenoid dysplasia, or osteoradionecrosis, or they are spontaneous. Spontaneous cephaloceles are often seen in obese middle-aged women with idiopathic intracranial hypertension, where the increased intracranial pressure, associated prominent arachnoid granulations, and progressive bony thinning are thought to lead to CSF leaks and herniation of the dura or brain.[63] Spontaneous cephaloceles and CSF leaks are typically seen in areas of thin bone including the cribriform plates, areas bordering the pneumatized paranasal sinuses, and the tegmen tympani.[63]

Imaging demonstrates a sac of fluid with or without brain tissue extending from the intracranial compartment through an osseous defect, with CT best demonstrating the bony defect and MR

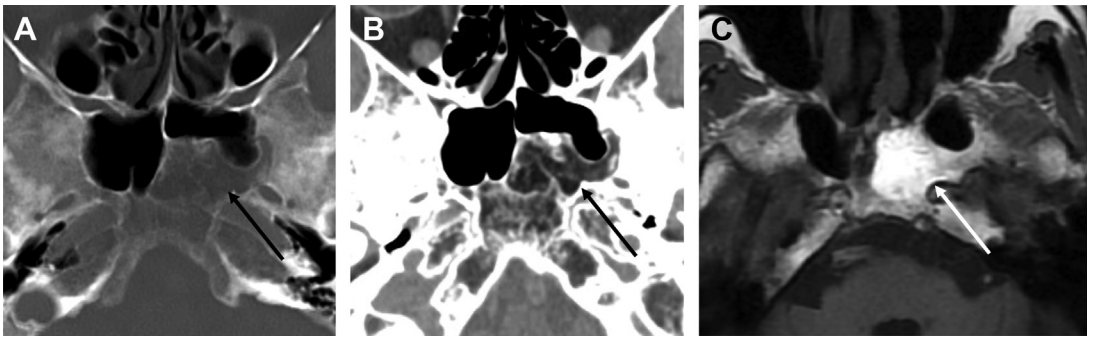

Fig. 6. Arrested pneumatization of the left sphenoid sinus. Axial CT images in bone (*A*) and soft tissue (*B*) windows show a well-circumscribed, well-corticated, lesion with internal curvilinear calcifications centered on a normal area of sphenoid pneumatization in the left sphenoid body (*arrows*). Soft tissue window demonstrates central fat density. Axial T1W MR image (*C*) shows the lesion demonstrates higher signal than the adjacent normal marrow within the clivus and sphenoid.

imaging best determining the contents of the cephalocele (**Fig. 7**). The sac and brain tissue may demonstrate heterogeneous enhancement. Cisternogram with intrathecal contrast administration may demonstrate leakage of contrast into the sac or into the surrounding tissues, as in the case of a CSF leak. On imaging, cephaloceles are mistaken for cystic or solid masses, therefore attention for skull base defects should be made for lesions bordering the skull base.

Cephaloceles can herniate into the paranasal sinuses, where they may be mistaken for mucoceles, polyps, or primary neoplasms on imaging and endoscopically.[62] When herniating into sinuses, they frequently present with CSF rhinorrhea but can also present with recurrent meningitis or, if large enough, airway obstruction.[53,62] Accurate diagnosis of cephaloceles is important because biopsy or resection runs a risk of iatrogenic intracranial infections, parenchymal contusion, or CSF leaks.[53] Surgical goals for these patients may include removal of the sac and any dysplastic brain tissue, preservation of any normal brain tissue, and secure closure of the wound.[56,57]

Fibrous Dysplasia

FD is a benign, slowly progressing, dysplastic process affecting osteogenesis, characterized by the replacement of normal medullary bone with abnormal fibrous tissue interspersed with irregularly shaped trabeculae of woven bone on histology.[64–67] It is thought to be caused by an activating missense mutation of the GNAS gene on chromosome 20, affecting the Gs protein alpha subunit and resulting in increased cAMP levels.[65,67,68] This mutation is seen in the areas of abnormal bone and in patients with McCune-Albright syndrome.

FD accounts for approximately 5% to 10% of all osseous tumors and has been classified with three main forms: (1) monostotic (80%); (2) polyostotic (20%); and (3) McCune-Albright syndrome, which is polyostotic disease with endocrine dysfunction, abnormal skin pigmentation, and precocious puberty.[64,65,67,68] Polyostotic disease can also be seen with other disorders, including primary hyperparathyroidism, tuberous sclerosis, and Mazabraud syndrome.[65,68] FD most commonly affects the craniofacial bones, in 10% to 25% of cases of monostotic disease and 50% to 100% of cases of polyostotic disease, predominantly affecting the ethmoid (71%), followed by the sphenoid (43%), frontal (33%), and maxilla (29%), with temporal bone involvement being rare.[67–70] Most patients with the disorder are asymptomatic, but presenting symptoms are usually related to the site of disease, such as facial asymmetry, sinusitis, vision loss from optic canal involvement, headache, hearing loss from temporal bone involvement, or facial pain.[65,67,69]

Imaging features of FD are variable and confusing. On CT, the intramedullary lesions are described as well-defined and expansile, with internal "ground-glass" density, cortical thinning, and endosteal scalloping, although lesions may also appear completely lucent or sclerotic. MR imaging features are nonspecific and depend on the amount of fibrous tissue present within the abnormal bone. They typically demonstrate intermediate signal intensity but may show higher T2 signal in lesions with less osseous trabeculation or more cystic change.[65,68] Lesions are highly vascular and can enhance intensely. Given the enhancement and variable MR imaging features, FD is often mistaken for skull base neoplasm on MR imaging. When MR imaging evaluation is equivocal, CT imaging may be helpful to evaluate for the characteristic internal "ground-glass" density (**Fig. 8**).

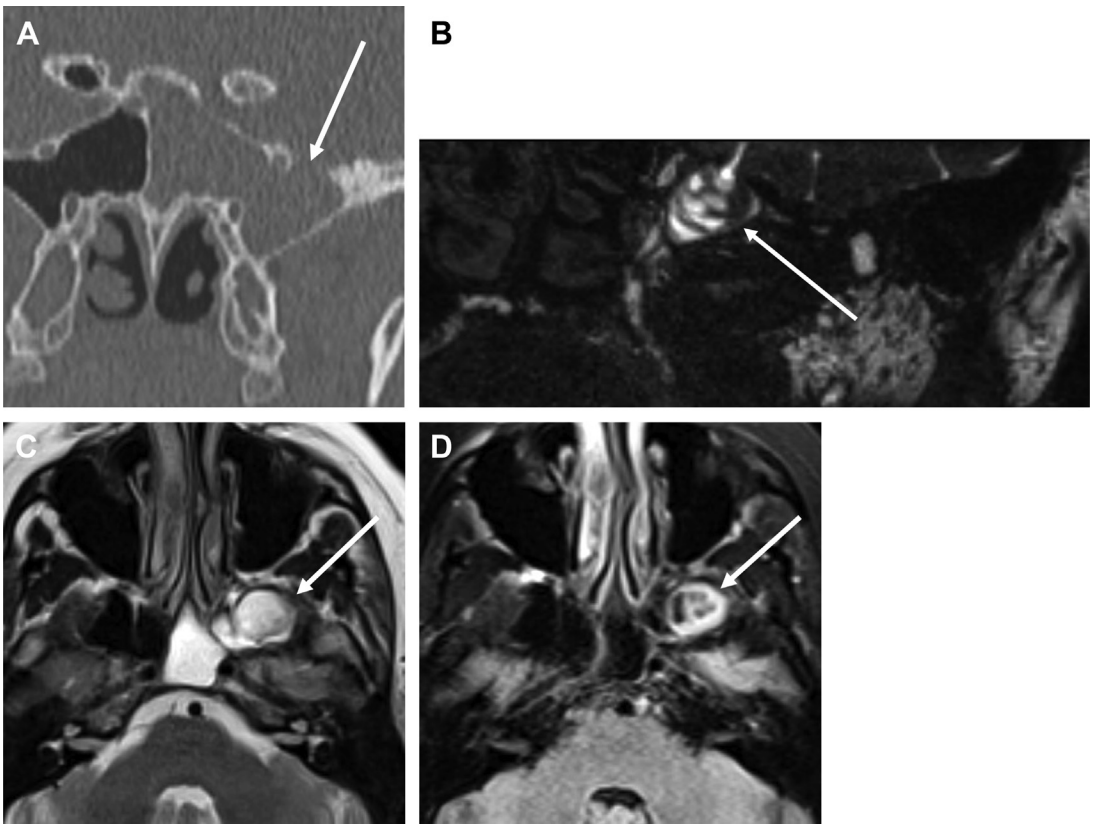

Fig. 7. Left greater sphenoid wing encephalocele. Coronal (*A*) CT image shows an osseous defect (*arrow*) through the left greater sphenoid wing with complete opacification of the left sphenoid sinus. Sagittal T2 SPACE (*B*), axial T2W (*C*), and axial contrast-enhanced T1W (*D*) MR images show abnormally enhancing herniated dysplastic, gliotic brain tissue extending from the adjacent temporal lobe into the left sphenoid sinus (*arrows*).

Imaging is clinically useful for evaluating for extent of disease and for rare complications of FD, including associated aneurysmal bone cyst formation, impingement on the optic nerve or temporal bone structures, and malignant degeneration.[65–69] Rapid expansion of the lesion, associated pain, bone destruction, or soft tissue invasion should raise suspicion for malignant degeneration, which occurs most commonly as osteosarcoma, fibrosarcoma, chondrosarcoma, or malignant fibrous histiocytosis.[65,66]

Ecchordosis Physaliphora

Ecchordosis physaliphora (EP) is a small, gelatinous benign, hamartomatous mass derived from remnant notochordal tissue, usually at midline along the dorsal wall of the clivus or in the sacrococcygeal region, although they can occur anywhere along the route of the notochord.[71–76]

EP are usually asymptomatic and found in 0.4% to 2.0% of autopsies.[72–78] They are usually intradural at the level of Dorello canal, attached to the dorsal wall of the clivus by an osseous stalk or pedicle. This contrasts with the related, rarer chordoma, a malignant neoplasm derived from notochordal remnant tissue, which is typically symptomatic, aggressive, and intraosseous, constituting 2% to 4% of primary bone tumors.[71,72,78] There have been case reports, however, of symptomatic EP with CSF fistulas into the sphenoid sinus, cervical spine EP resulting in hemiparesis and hemihypoesthesia, spontaneous pneumocephalus and pneumoventricle, headache, abducens nerve palsy, intracranial hypertension, intratumoral hemorrhage, CSF rhinorrhea, meningitis, and spontaneous rupture resulting in recurrent pneumocephalus and presenting as imbalance, headache, and rhinorrhea.[77,79–86]

Regarding imaging features of EP, CT imaging is generally limited and may only be useful for assessing for an associated osseous stalk arising from the clivus or confirming smooth well-defined bony margins. MR imaging is more helpful, with EP typically appearing as a homogeneous, T1 hypointense, T2 hyperintense, well-circumscribed, midline mass along the dorsal wall of the clivus (**Fig. 9**).[72–75,77,79] Given the

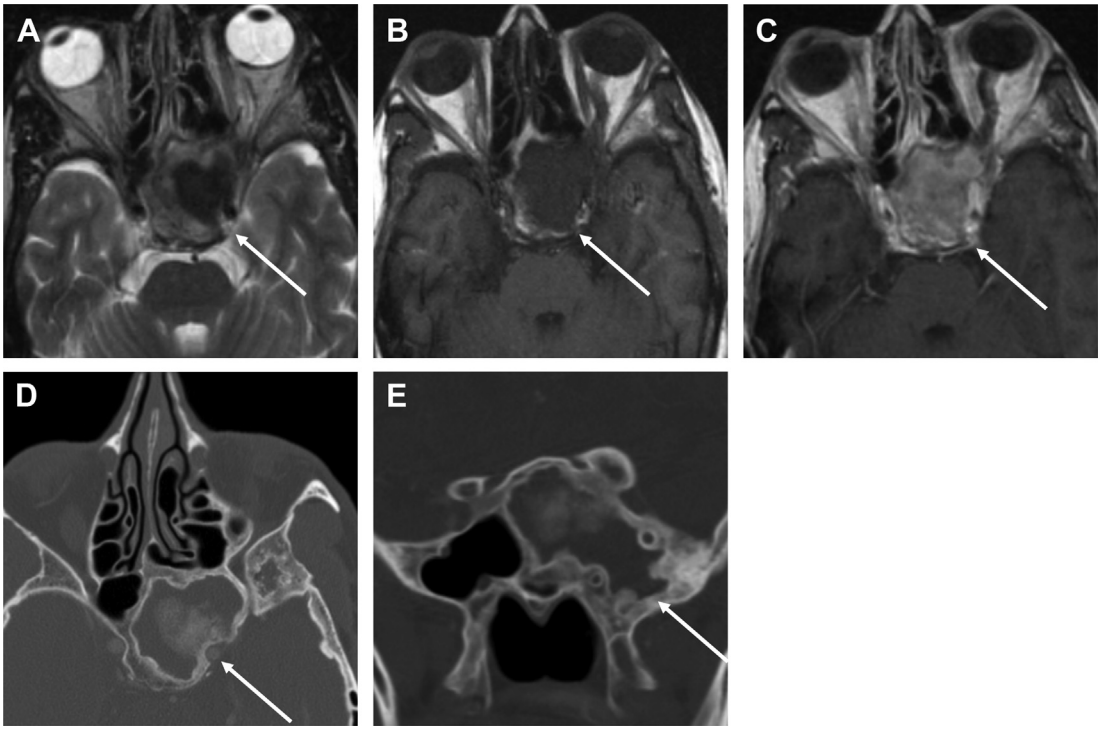

Fig. 8. Left sphenoid body fibrous dysplasia. Axial T2W (*A*), T1W (*B*), and T1W contrast-enhanced (*C*) MR images demonstrate a lobulated T2 heterogeneous, T1 hypointense, enhancing lesion in the left sphenoid body (*arrows*). The MR imaging appearance mimics a malignant neoplasm. Axial (*D*) and coronal (*E*) CT images demonstrate an expansile lesion with preservation of the cortices and internal ground-glass density (*arrows*) compatible with fibrous dysplasia. Note the predominant lucent component, which can be seen with fibrous dysplasia.

location and signal characteristics of EP, it can be mistaken for lesions such as chordoma, chondrosarcoma, or metastasis, but EP should not demonstrate any aggressive, bony destructive features. EP typically also does not demonstrate contrast enhancement, whereas chordoma typically avidly enhances.[72–75,77,78,83] Any bony destruction, inhomogeneous signal characteristics, loculations, or contrast enhancement should raise suspicion for a malignant pathology. There have been case reports of enhancing EP and nonenhancing chordoma, however, so contrast enhancement characteristics are not entirely reliable, and imaging follow-up is generally recommended.[74]

Invasive and Ectopic Pituitary Adenoma

Pituitary adenomas are the most common lesions found in the sella turcica and among the most common primary brain tumors overall, accounting for 10% to 15% of primary brain tumors.[87,88] Most pituitary adenomas remain confined to the sellar space, but large invasive pituitary adenomas (IPA) may demonstrate extrasellar extension, often extending into the suprasellar space or cavernous sinuses.[89–92] Uncommonly, large pituitary adenomas can demonstrate infrasellar extension, involving the clivus, sphenoid sinus, and even the pharynx, petrosal sinus, jugular foramen, or hypoglossal canal.[87,88,90,92–94] Given the location and invasive features of the IPA, these lesions are mistaken for more aggressive skull base neoplasms, such as chordoma, chondrosarcoma, meningioma, astrocytoma, craniopharyngioma, or metastases.[87,88,93]

Pituitary adenomas may also rarely be ectopic in location and can arise anywhere along the course of Rathke pouch as it extends to the sella turcica in utero.[87,88,95,96] They are most common in the sphenoid sinus, although they are also seen in the nasopharynx, cavernous sinus, and uncommonly in the clivus. When occurring in the skull base or other ectopic locations, these can also be mistaken for neoplasm.

On imaging, IPA typically demonstrates smooth enlargement of the sella turcica and when invading the cavernous sinus, it typically encases the cavernous internal carotid artery (ICA) without associated vascular narrowing (**Fig. 10**). Various imaging features may help to differentiate pituitary adenoma from malignant neoplasms, such as lower T2 signal, more avid enhancement, and lower apparent diffusion coefficient of IPA when

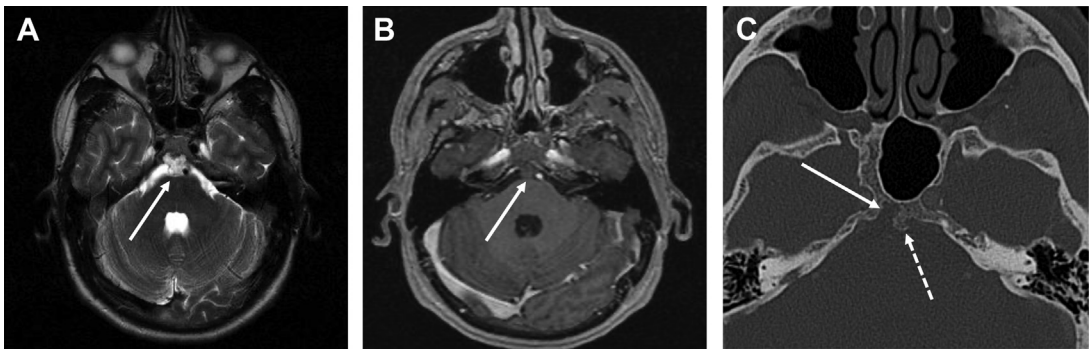

Fig. 9. Ecchordosis physaliphora. Axial T2W (*A*) and T1W contrast-enhanced (*B*) MR images show a small, well-circumscribed, nonenhancing lesion within the dorsal clivus extending into the prepontine cistern (*arrows*). Axial CT image (*C*) in a different patient demonstrates a well-defined lobulated defect in the right aspect of the clivus (*solid arrow*) with an osseous stalk extending posteriorly from the midline clivus (*dashed arrow*).

compared with chordoma and other malignant processes.[93] Atypical features for IPA, such as enlargement of the pituitary stalk, rapid growth, clival or sellar destruction, or luminal narrowing of the ICA when cavernous sinus invasion is present, should point away from IPA.[97] Sellar enlargement occurs in nearly 100% of pituitary macroadenomas, and although it is also seen in nonadenomatous masses, its absence, or the presence of erosion without enlargement, is suggestive of other neoplasms.[98]

Skull Base Osteomyelitis and Inflammatory Processes

Given the complexity of the skull base and its surrounding structures, there are a multitude of infectious and inflammatory processes that can present with confusing clinical and imaging characteristics. For example, inflammatory pseudotumor (IPT), granulomatosis with polyangiitis, sarcoidosis, IgG4-related sclerosing disease, osteomyelitis, fungal sinusitis, and Langerhans cell histiocytosis may all have varied and nonspecific clinical and imaging findings, creating diagnostic difficulty and often requiring biopsy to differentiate them from chordoma, chondrosarcoma, nasopharyngeal carcinoma, or metastases.[99]

Skull base osteomyelitis (SBO) involving the cranial vault or skull base is rare, with the incidence of SBO higher in developing countries, thought likely to be related to lower antibiotic use.[100–103] Recent history of an otogenic or sinonasal infection, fever, or leukocytosis in at-risk elderly patients with diabetes or immunocompromised patients can help suggest this diagnosis.[100,101,103] Symptoms, however, may be nonspecific, with an insidious and delayed onset of symptoms, such as headache and facial pain, with presentation starting many weeks after resolution of an initial otogenic or sinonasal infection.[101–103] This can lead to delays in diagnosis, and diagnosis might only be made after onset of neurologic deficits from cranial nerve involvement or compression, which carries a worse prognosis.[102,103]

On imaging, SBO may appear as a soft tissue mass with bone erosion or demineralization and inflammatory changes on CT, although it is often occult in its early stages. MR imaging is more

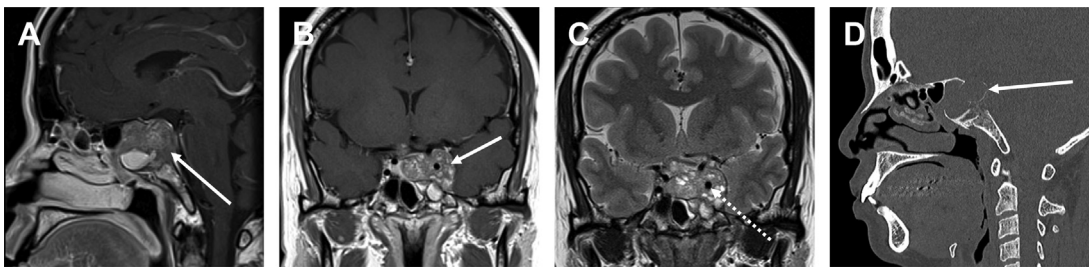

Fig. 10. Invasive pituitary adenoma. Sagittal (*A*) contrast-enhanced MR image demonstrates a heterogeneously enhancing mass (*arrow*) in the central skull base with no identifiable separate pituitary tissue. Coronal contrast-enhanced T1W (*B*) and T2W (*C*) MR images demonstrate invasion of the left cavernous sinus (*solid arrow*) and encasement of the cavernous left ICA (*dashed arrow*), without associated vascular narrowing, characteristic for a pituitary adenoma. Sagittal CT image (*D*) demonstrates smooth remodeling and expansion of the central skull base by the adenoma (*arrow*).

useful for evaluating the extent of the disease, appearing as an infiltrative, hypointense mass on T1-weighted (T1W) images that demonstrates contrast enhancement and surrounding inflammation (**Fig. 11**). It demonstrates variable signal intensity on T2-weighted (T2W) images, with hypointense signal thought to be related to the chronicity of the inflammatory process and the degree of fibrosis.[102,103] SBO may demonstrate reduced diffusion, particularly in areas of abscess formation.[104] Delayed diagnosis of SBO can also lead to complications, such as intracranial spread, arterial involvement and infarct, pseudoaneurysm, and venous sinus thrombosis.[101] Biopsy is often necessary to guide treatment, because SBO may be treated with long-term antibiotics or conservative surgery, differing from inflammatory or malignant processes.[100]

IPT, also known as plasma cell granuloma or myofibroblastic pseudotumor, is a benign, inflammatory process demonstrating acute and chronic inflammatory cells and fibrosis on histopathology.[105,106] Many patients also exhibit elevated serum IgG4 levels and IgG4-positive plasma cells on pathology, suggesting that some IPT may reflect a manifestation of IgG4-related sclerosing disease.[105,107,108] Although it most commonly occurs in the orbit, it can involve other areas, including the brain, cavernous sinus, nasopharynx, and skull base.[105,106,109] On MR imaging, it appears as an infiltrative enhancing mass; marked T2 hypointensity is suggestive of IPT and other chronic inflammatory processes. MR imaging can help evaluate for cranial nerve compression or involvement, which can result in cranial nerve palsies, pain, vision changes, or hearing loss.[105–110] IPT is generally treated with steroids and/or radiation therapy.[105]

Granulomatosis with polyangiitis is an autoimmune vasculitis involving small and medium sized vessels, characterized by necrotizing granulomatous inflammation of the respiratory tracts and necrotizing glomerulonephritis.[111] Although granulomatosis with polyangiitis is thought of as a disease of the respiratory tracts and kidneys that can spread systemically to involve any organ, 10% of patients present initially with isolated skull base disease causing cranial neuropathies.[111–113] It may appear as a diffuse, infiltrative enhancing mass involving the skull base and surrounding soft tissues; like IPT, marked T2W hypointensity can suggest a chronic inflammatory process not typically seen with neoplasm (**Fig. 12**). Clinical history, laboratory evaluation of serum antineutrophil cytoplasmic antibodies, and possibly tissue sampling are key for accurate diagnosis and appropriate treatment. Treatment may involve steroids or cytotoxic agents.[112–114]

PETROUS APEX

The petrous apex is a small region of the skull base with complex anatomy, lending itself to involvement by a variety of different pathologies.[115–117] Petrous apex lesions are generally characterized as operative (neoplastic or inflammatory) or nonoperative (incidental), with most nonneoplastic lesions occurring as a result of air cell disease, such as cholesterol granuloma, cholesteatoma, or mucocele.[115] The petrous apex is difficult to clinically evaluate because of its depth, thus imaging is important for differentiation between operative and nonoperative lesions to guide management.

Petrous Apex Cephalocele

Petrous apex cephalocele (PAC) is a rare congenital or acquired lesion characterized by herniation of dura mater or arachnoid from the posterolateral portion of Meckel cave into the anterior petrous apex.[115–117] It may reflect a meningocele or arachnoid cyst. On CT, it appears as a homogeneously hypoattenuating, fluid density, circumscribed, well-corticated lesion extending from Meckel

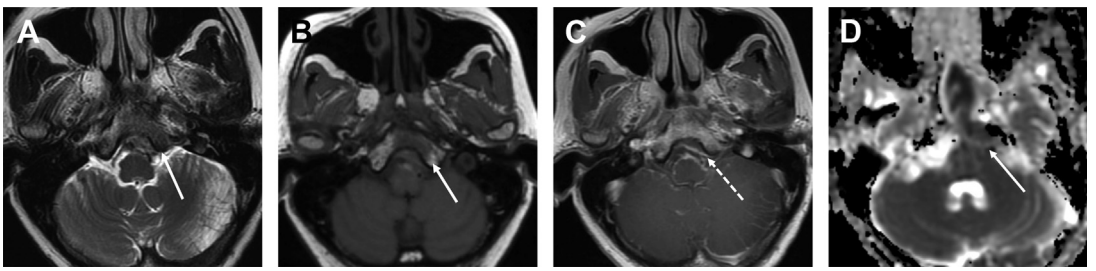

Fig. 11. Skull base osteomyelitis arising from sphenoid sinusitis. Axial T2W (*A*) and T1W (*B*) MR images show ill-defined hypointensity within the clivus (*arrows*). Axial contrast-enhanced T1W MR image (*C*) shows enhancement of the area and leptomeningeal enhancement and rim enhancement around an epidural abscess, reflecting intracranial spread (*dashed arrow*). Apparent diffusion coefficient map (*D*) shows reduced diffusion within the affected skull base and the epidural collection (*arrow*).

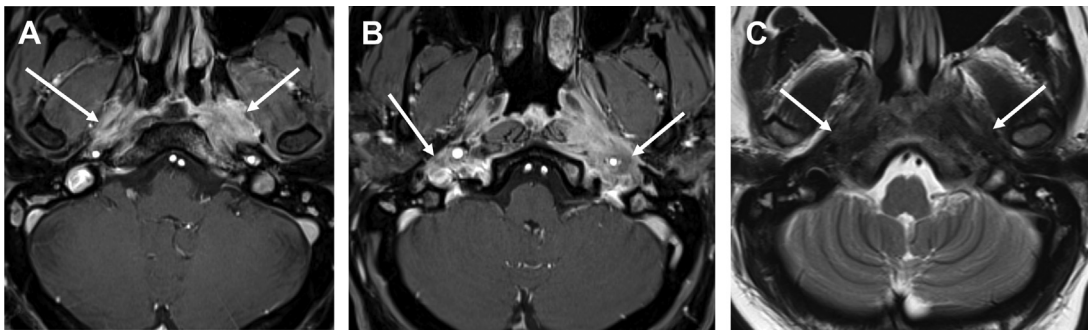

Fig. 12. Skull base granulomatosis with polyangiitis. Axial contrast-enhanced T1W fat-saturated (*A* and *B*) and T2W (*C*) MR images demonstrate ill-defined enhancement in the left greater than right parapharyngeal and carotid spaces (*arrows*), clivus, and surrounding soft tissues. Note the marked hypointense signal on T2W images suggesting chronic inflammatory tissue.

cave and eroding into the anterior petrous apex.[115–117] On MR imaging, it follows fluid signal and can contain traversing trigeminal nerve fibers (**Figs. 13** and **14**). They may have a mildly enhancing thin wall, but they do not demonstrate reduced diffusion.[115,117]

Most PACs are asymptomatic and incidentally found, but when symptomatic they may present with headache, CSF rhinorrhea, CSF leak, trigeminal neuralgia, or symptoms of intracranial hypertension.[115,117] They are usually unilateral, but can be bilateral.[61,115,117] The exact cause of PAC is not definitely known, but it may be caused by altered CSF dynamics resulting in intracranial hypertension, with herniation of the meninges into the petrous apex occurring as a natural pathway to alleviate pressure.[115,117] This is supported by the association of PAC with symptoms of intracranial hypertension and with imaging evidence of empty sella in up to 69%.[117]

Asymmetric Pneumatization of the Petrous Apex

Although most petrous apices are filled with normal fatty marrow, they are pneumatized in up to 35%.[118,119] Pneumatization of the petrous apices is usually bilateral and symmetric but is asymmetric in 4%.[118,120] When the petrous apices are asymmetrically pneumatized, with one nonpneumatized or underpneumatized, the normal high signal of the marrow on T1W images of the nonpneumatized petrous apex is mistaken for cholesterol granulomas or misinterpreted as enhancement.[118] It does, however, suppress on

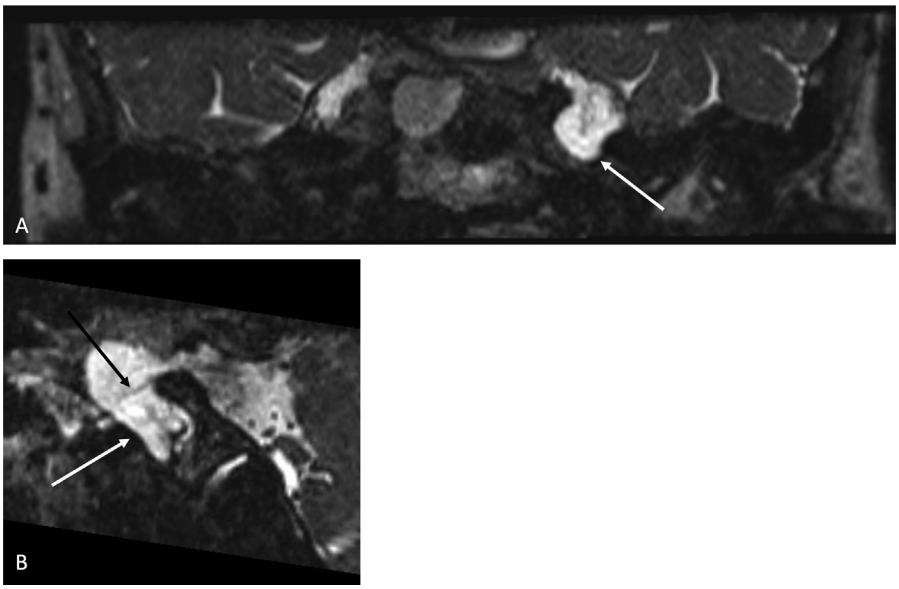

Fig. 13. Left petrous apex cephalocele. Coronal (*A*) and sagittal (*B*) T2 SPACE MR images show a circumscribed left petrous apex cephalocele extending from the posterior aspect of Meckel cave into the left petrous apex (*white arrows*). There are traversing trigeminal nerve fibers extending into the cephalocele (*black arrow*).

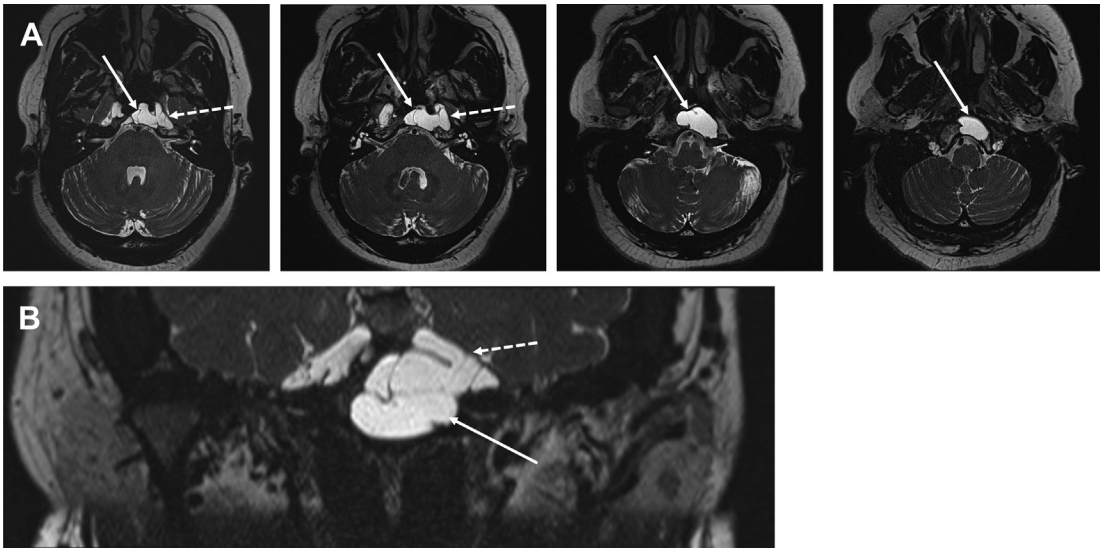

Fig. 14. Left petrous apex cephalocele. Axial (*A*) and coronal (*B*) T2 SPACE MR images demonstrate a homogeneous, well-circumscribed, lesion following CSF signal in the petrous apex and clivus (*solid arrows*), continuous with the inferior aspect of the left Meckel cave (*dashed arrows*). This was initially misinterpreted as a skull base neoplasm.

fat-suppressed imaging and it does not expand the petrous apex or exhibit reduced diffusion.[116,118,120] CT imaging can further elucidate the diagnosis by demonstrating normal marrow and cortex of the nonpneumatized petrous apex (**Fig. 15**).

Petrous Apex Effusion

In addition to misinterpretation of the nonpneumatized petrous apex, a fluid-filled pneumatized petrous apex may also be mistaken for pathologies, such as petrous apicitis, congenital cholesteatoma, cholesterol granuloma, or tumor. Petrous apex effusions appear hyperintense on T2W images, with variable signal on T1W images thought to be caused by variable amounts of protein content within the trapped fluid, with preservation of the bony septations and cortex on CT (**Fig. 16**).[119,121,122] Cholesterol granulomas, in contrast, present symptomatically with intrinsic T1 hyperintensity on MR imaging and bony expansion and loss of the normal osseous trabeculae/septations on CT images (**Fig. 17**).[119,122] Patients with petrous apicitis also usually present symptomatically, and imaging demonstrates surrounding inflammation, osseous erosions, and fluid within the middle ear and mastoid air cells.[118]

Petrous Internal Carotid Artery Aneurysm

Aneurysms of the extradural ICA are rare, and aneurysms of the petrous segment of the extradural ICA are extremely rare, usually found incidentally.[123–127] When patients are symptomatic from petrous ICA aneurysms, they commonly

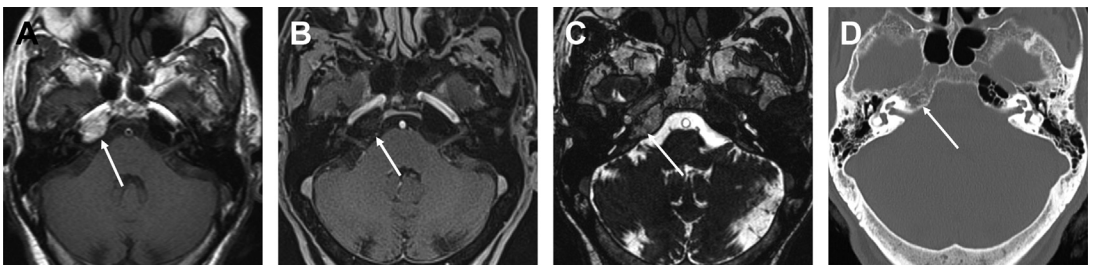

Fig. 15. Asymmetric pneumatization of the left petrous apex. Axial T1W (*A*), contrast-enhanced T1W fat-saturated (*B*), and T2 SPACE (*C*) MR images demonstrate a well-circumscribed, T1 hyperintense, nonexpansile lesion in the right petrous apex (*arrows*), which suppresses on the fat-saturated sequence. The T1 hyperintensity was confused for a cholesterol granuloma. Axial CT image (*D*) demonstrates normal marrow characteristics in the right petrous apex (*arrow*), appearing similar to the adjacent clivus, with preservation of the cortex, and a pneumatized left petrous apex.

Fig. 16. Right petrous apex effusion. Axial (*A*) and coronal (*B*) T2W MR images show T2 hyperintense signal within the right petrous apex (*arrows*). Axial T1W MR image (*C*) shows corresponding intermediate to hyperintense signal (*arrow*). A follow-up axial CT image (*D*) shows a pneumatized right petrous apex with fluid, with preservation of the septations and cortex. There are a few foci of antidependent air along the anterior portion of the petrous apex (*dashed arrow*).

present with cranial nerve symptoms resulting from mass effect of the aneurysm, but they may also present with headache, Horner syndrome, pulsatile tinnitus, sensorineural hearing loss, thromboembolic events, cavernous sinus syndrome, or life-threatening otorrhagia or epistaxis.[123–125,128–131]

On CT, they appear as slightly hyperattenuating masses expanding and scalloping the petrous apex. They may also exhibit peripheral thrombus or wall calcifications. On MR imaging, they may exhibit a variety of appearances depending on the presence of thrombus, slow flow, or turbulent flow. If the aneurysm has a significant amount of

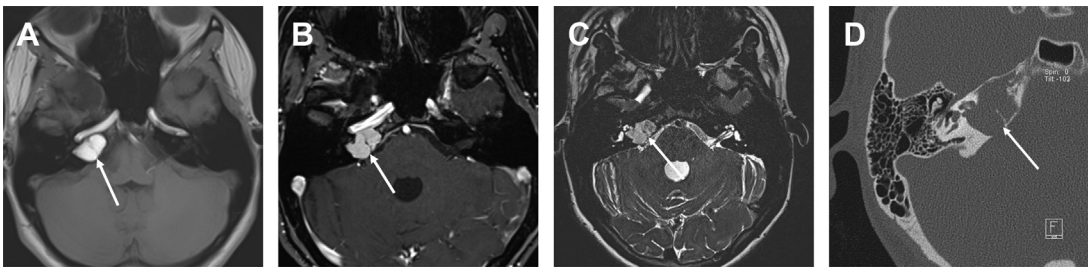

Fig. 17. Right petrous apex cholesterol granuloma. Axial T1W (*A*), contrast-enhanced fat-suppressed T1W (*B*), and T2 SPACE (*C*) MR images demonstrate a well-circumscribed, homogeneous, intrinsically T1 hyperintense lesion in the right petrous apex without obvious enhancement (*arrow*). Axial CT image (*D*) demonstrates a lucent, expansile, well-circumscribed lesion (*arrow*) with loss of the central septations.

Fig. 18. Right petrous ICA aneurysm. Axial noncontrast CT image (*A*) and axial (*B*) and coronal (*C*) maximum intensity projection CT angiogram images demonstrate a hyperdense, well-circumscribed, homogeneous, arterially enhancing saccular outpouching (*arrows*) arising from the petrous ICA and extending superiorly through a defect in the petrous part of the temporal bone into the middle cranial fossa. (*Courtesy of* G. Moonis, MD, New York, New York).

flow, they may demonstrate a flow void within the central portion of the aneurysm. Turbulent flow may appear as more heterogeneous, intermediate signal on T1W and T2W images, and slow flow or thrombosis may appear as a soft tissue mass and demonstrate homogeneous enhancement.[116,123,124] Given the varied imaging characteristics, these can be mistaken for chondrosarcoma, invasive meningioma, or metastases. One clue to look for is the presence of vascular pulsation artifacts propagating from the aneurysm along the phase-encoding direction. Care must be taken to prevent inadvertent biopsies or resections of these aneurysms. CT angiography, MR angiography, or conventional angiogram should also be obtained to confirm the diagnosis, evaluate the aneurysm neck, and assess the context of the aneurysm with regards to the parent vessel and adjacent neurovascular structures for endovascular or surgical planning (**Fig. 18**).

If left untreated, these aneurysm are associated with a high rate of thromboembolic events, seen in up to 50% of patients.[123] Because the petrous ICA aneurysms are often completely enclosed by bone, surgical access for ligation is difficult and endovascular therapy is the preferred approach.[123,124,126] This is performed with a variety of techniques, such as flow-diverting stent placement, coil embolization, or progressive flow reduction.

SUMMARY

The skull base features complex anatomy, containing many different tissue types, foramina, canals, and synchondroses, predisposing it to a variety of anatomic variants and masses, benign and malignant. Skull base lesions can demonstrate a variety of confusing appearances on imaging, creating diagnostic dilemmas. It is important to be familiar with imaging appearances of common mimickers of malignant neoplasm in the skull base to be able to accurately diagnose them and prevent unnecessary imaging follow-up, biopsies, or interventions.

CLINICS CARE POINTS

- Familiarity with the common normal variant and benign lesions occurring in the skull base may prevent confusion with more sinister pathologies, reducing healthcare waste and patient stress.
- Anatomic variants in the skull base are common, occurring along the course of the notochord and craniopharyngeal canal.
- Ill-defined hypointensity on T2 with surrounding inflammatory changes can suggest skull base osteomyelitis or chronic inflammatory process.
- Petrous internal carotid artery aneurysm is a "must not miss" diagnosis with varied imaging appearances on MRI depending on the flow and amount of thrombus formation.
- Other benign mimics in the skull base have characteristic appearances, including arrested pneumatization of the sphenoid sinus, cephalocele, fibrous dysplasia, ecchordosis physaliphora, and invasive pituitary adenoma.

DISCLOSURES

The authors have nothing to disclose.

REFERENCES

1. Raut A, Naphade P, Chawla A. Imaging of skull base: pictorial essay. Indian J Radiol Imaging 2012;22:305.

2. Borges A. Imaging of the central skull base. Neuroimaging Clin N Am 2009;19:441–68.
3. Thust SC, Yousry T. Imaging of skull base tumours. Rep Pract Oncol Radiother 2016;21:304–18.
4. Kunimatsu A, Kunimatsu N. Skull base tumors and tumor-like lesions: a pictorial review. Pol J Radiol 2017;82:398–409.
5. Currarino G. Canalis basilaris medianus and related defects of the basiocciput. AJNR Am J Neuroradiol 1988;9:208–11.
6. Jacquemin C, Bosley TM, al Saleh M, et al. Canalis basilaris medianus: MRI. Neuroradiology 2000;42:121–3.
7. Hughes ML, Carty AT, White FE. Persistent hypophyseal (craniopharyngeal) canal. Br J Radiol 1999;72:204–6.
8. Abele TA, Salzman KL, Harnsberger HR, et al. Craniopharyngeal canal and its spectrum of pathology. Am J Neuroradiol 2014;35:772–7.
9. Zhang WH, Yen WC. A new bony canal on the clival surface of the occipital bone. Acta Anat (Basel) 1987;128:63–6.
10. Syed AZ, Zahedpasha S, Rathore SA, et al. Evaluation of canalis basilaris medianus using cone-beam computed tomography. Imaging Sci Dent 2016;46:141–4.
11. Bayrak S, Göller Bulut D, Orhan K. Prevalence of anatomical variants in the clivus: fossa navicularis magna, canalis basilaris medianus, and craniopharyngeal canal. Surg Radiol Anat 2019;41:477–83.
12. Madeline LA, Elster AD. Postnatal development of the central skull base: normal variants. Radiology 1995;196:757–63.
13. Paraskevas GK, Tsitsopoulos PP, Ioannidis OM. Incidence and purpose of the clival canal, a "neglected" skull base canal. Acta Neurochir (Wien) 2013;155:139–40.
14. Tubbs RS, Griessenauer CJ, Loukas M, et al. The enigmatic clival canal: anatomy and clinical significance. Childs Nerv Syst 2010;26:1207–10.
15. Jalšovec D, Vinter I. Clinical significance of a bony canal of the clivus. Eur Arch Otorhinolaryngol 1999; 256:160–1.
16. Nguyen RP, Salzman KL, Stambuk HE, et al. Extraosseous chordoma of the nasopharynx. Am J Neuroradiol 2009;30:803–7.
17. Martinez CR, Hemphill JM, Hodges FJ, et al. Basioccipital meningocele. AJNR Am J Neuroradiol 1981;2:100–2.
18. Hemphill M, Freeman JM, Martinez CR, et al. A new, treatable source of recurrent meningitis: basioccipital meningocele. Pediatrics 1982;70:941–3.
19. Morabito R, Longo M, Rossi A, et al. Pharyngeal enterogenous cyst associated with canalis basilaris medianus in a newborn. Pediatr Radiol 2013; 43:512–5.
20. Lohman BD, Sarikaya B, McKinney AM, et al. Not the typical Tornwaldt's cyst this time? A nasopharyngeal cyst associated with canalis basilaris medianus. Br J Radiol 2011;84:e169–71.
21. Khairy S, Almubarak AO, Aloraidi A, et al. Canalis basalis medianus with cerebrospinal fluid leak: rare presentation and literature review. Br J Neurosurg 2019;33:432–3.
22. Ko AL, Gabikian P, Perkins JA, et al. Endoscopic repair of a rare basioccipital meningocele associated with recurrent meningitis: case report. J Neurosurg Pediatr 2010;6:188–92.
23. Syed AZ, Mupparapu M. Fossa navicularis magna detection on cone-beam computed tomography. Imaging Sci Dent 2016;46(1):47–51.
24. Beltramello A, Puppini G, El-Dalati G, et al. Fossa navicularis magna. AJNR Am J Neuroradiol 1998;19: 1796–8.
25. Ray B, Kalthur S, Kumar B, et al. Morphological variations in the basioccipital region of the South Indian skull. Nepal J Med Sci 2015;3:124–8.
26. Cankal F, Ugur HC, Tekdemir I, et al. Fossa navicularis: anatomic variation at the skull base. Clin Anat 2004;17:118–22.
27. Ersan N. Prevalence and morphometric features of fossa navicularis on cone beam computed tomography in Turkish population. Folia Morphol 2017;76:6.
28. Ginat DT, Ellika SK, Corrigan J. Multidetector-row computed tomography imaging of variant skull base foramina. J Comput Assist Tomogr 2013;37:5.
29. Prabhu SP, Zinkus T, Cheng AG, et al. Clival osteomyelitis resulting from spread of infection through the fossa navicularis magna in a child. Pediatr Radiol 2009;39:995–8.
30. Alalade AF, Briganti G, Mckenzie J-L, et al. Fossa navicularis in a pediatric patient: anatomical skull base variant with clinical implications. J Neurosurg Pediatr 2018;22:523–7.
31. Segal N, Atamne E, Shelef I, et al. Intracranial infection caused by spreading through the fossa naviclaris magna: a case report and review of the literature. Int J Pediatr Otorhinolaryngol 2013;77:1919–21.
32. Currarino G, Maravilla KR, Salyer KE. Transsphenoidal canal (large craniopharyngeal canal) and its pathologic implications. AJNR Am J Neuroradiol 1985;6:39–43.
33. Arey LB. The craniopharyngeal canal reviewed and reinterpreted. Anat Rec 1950;106:1–16.
34. Larsen JL, Bassøe HH. Transsphenoidal meningocele with hypothalamic insufficiency. Neuroradiology 1979;18:205–9.
35. Hori A, Schmidt D, Rickels E. Pharyngeal pituitary: development, malformation, and tumorigenesis. Acta Neuropathol 1999;98:262–72.
36. Hooper AC. Sphenoidal defects: a possible cause of cerebrospinal fluid rhinorrhoea. J Neurol Neurosurg Psychiatry 1971;34:739–42.
37. Rajasekar G, Nair P, Abraham M, et al. Endoscopic endonasal repair of a persistent craniopharyngeal

canal and sphenoid meningoencephalocele: case report and review of literature. World Neurosurg 2019;122:196–202.
38. Lingappa L, Konanki R, Varma R, et al. Persistent craniopharyngeal canal: a rare cause for recurrent meningitis in pediatric population. Ann Indian Acad Neurol 2019;0:0.
39. Habermann S, Silva AHD, Aquilina K, et al. A persistent craniopharyngeal canal with recurrent bacterial meningitis: case report and literature review. Childs Nerv Syst 2021;37:699–702.
40. Poonia SK, Cazzador D, Kaufman AC, et al. Disorders involving a persistent craniopharyngeal canal: a case series. J Neurol Surg B Skull Base 2020;81:562–6.
41. Kaushik C, Ramakrishnaiah R, Angtuaco EJ. Ectopic pituitary adenoma in persistent craniopharyngeal canal: case report and literature review. J Comput Assist Tomogr 2010;34:612–4.
42. Ekinci G, Kiliç T, Baltacioğlu F, et al. Transsphenoidal (large craniopharyngeal) canal associated with a normally functioning pituitary gland and nasopharyngeal extension, hyperprolactinemia, and hypothalamic hamartoma. Am J Roentgenol 2003;180:76–7.
43. Kumar S, Pujari VS, Munshi M, et al. Neonatal respiratory distress produced by a nasopharyngeal glioma with a persistent craniopharyngeal canal. J Med Imaging Radiat Oncol 2020;64:824–6.
44. Chen CJ. Suprasellar and infrasellar craniopharyngioma with a persistent craniopharyngeal canal: case report and review of the literature. Neuroradiology 2001;43:760–2.
45. Welker KM, DeLone DR, Lane JI, et al. Arrested pneumatization of the skull base: imaging characteristics. Am J Roentgenol 2008;190:1691–6.
46. Scuderi AJ, Harnsberger HR, Boyer RS. Pneumatization of the paranasal sinuses: normal features of importance to the accurate interpretation of CT scans and MR images. Am J Roentgenol 1993;160:1101–4.
47. Spaeth J, Krügelstein U, Schlöndorff G. The paranasal sinuses in CT-imaging: development from birth to age 25. Int J Pediatr Otorhinolaryngol 1997;39:25–40.
48. Yonetsu K, Watanabe M, Nakamura T. Age-related expansion and reduction in aeration of the sphenoid sinus: volume assessment by helical CT scanning. AJNR Am J Neuroradiol 2000;21(1):179–82. [Epub ahead of print].
49. Shah RK, Dhingra JK, Carter BL, et al. Paranasal sinus development: a radiographic study. Laryngoscope 2003;113:205–9.
50. Jalali E, Tadinada A. Arrested pneumatization of the sphenoid sinus mimicking intraosseous lesions of the skull base. Imaging Sci Dent 2015;45:67–72.
51. Arpaci T. Arrested pneumatization of the sphenoid sinus mimicking skull base tumours: MRI prevalence in children with haematologic diseases. Int J Neurosci 2018;128:1040–3.
52. Tuncay OC, Ho D, Barker MK. Oxygen tension regulates osteoblast function. Am J Orthod Dentofacial Orthop 1994;105:457–63.
53. Nager GT. Cephaloceles. Laryngoscope 1987;97:77–84.
54. Simpson DA, David DJ, White J. Cephaloceles: treatment, outcome, and antenatal diagnosis. Neurosurgery 1984;15:14–21.
55. Baradaran N, Nejat F, Baradaran N, et al. Cephalocele: report of 55 cases over 8 years. Pediatr Neurosurg 2009;45:461–6.
56. Lo BWY, Kulkarni AV, Rutka JT, et al. Clinical predictors of developmental outcome in patients with cephaloceles: clinical article. J Neurosurg Pediatr 2008;2:254–7.
57. Martínez-Lage JF, Poza M, Sola J, et al. The child with a cephalocele: etiology, neuroimaging, and outcome. Childs Nerv Syst 1996;12(9):540–50.
58. Budorick NE, Pretorius DH, McGahan JP, et al. Cephalocele detection in utero: sonographic and clinical features. Ultrasound Obstet Gynecol 1995;5:77–85.
59. Brown MS, Sheridan-Pereira M. Outlook for the child with a cephalocele. Pediatrics 1992;90:914–9.
60. Wininger SJ, Donnenfeld AE. Syndromes identified in fetuses with prenatally diagnosed cephaloceles. Prenat Diagn 1994;14:839–43.
61. Alkhaibary A, Musawnaq F, Almuntashri M, et al. Bilateral petrous apex cephaloceles: is surgical intervention indicated? Int J Surg Case Rep 2020;72:373–6.
62. Deasy NP, Jarosz JM, Sarraj SA, et al. Intrasphenoid cephalocele: MRI in two cases. Neuroradiology 1999;41:497–500.
63. Alonso RC, de la Peña MJ, Caicoya AG, et al. Spontaneous skull base meningoencephaloceles and cerebrospinal fluid fistulas. RadioGraphics 2013;33:553–70.
64. Lustig LR, Holliday MJ, McCarthy EF, et al. Fibrous dysplasia involving the skull base and temporal bone. Arch Otolaryngol Neck Surg 2001;127:1239.
65. Schreiber A, Villaret AB, Maroldi R, et al. Fibrous dysplasia of the sinonasal tract and adjacent skull base. Curr Opin Otolaryngol Head Neck Surg 2012;20:45–52.
66. Fitzpatrick KA, Taljanovic MS, Speer DP, et al. Imaging findings of fibrous dysplasia with histopathologic and intraoperative correlation. Am J Roentgenol 2004;182:1389–98.
67. Amit M, Fliss DM, Gil Z. Fibrous dysplasia of the sphenoid and skull base. Otolaryngol Clin North Am 2011;44:891–902.
68. Kushchayeva YS, Kushchayev SV, Glushko TY, et al. Fibrous dysplasia for radiologists: beyond

ground glass bone matrix. Insights Imaging 2018; 9:1035–56.
69. Brown EW, Megerian CA, McKenna MJ, et al. Fibrous dysplasia of the temporal bone: imaging findings. Am J Roentgenol 1995;164:679–82.
70. Chong VFH, Khoo JBK, Fan Y-F. Fibrous dysplasia involving the base of the skull. Am J Roentgenol 2002;178:717–20.
71. Windeyer BW. Chordoma. Proc R Soc Med 1959; 52:1088–100.
72. Mehnert F, Beschorner R, Kuker W, et al. Retroclival ecchordosis physaliphora: MR imaging and review of the literature. AJNR Am J Neuroradiol 2004; 25(10):1851–5. [Epub ahead of print].
73. Watanabe A, Yanagita M, Ishii R, et al. Magnetic resonance imaging of ecchordosis physaliphora–case report. Neurol Med Chir (Tokyo) 1994;34: 448–50.
74. Park HH, Lee K-S, Ahn SJ, et al. Ecchordosis physaliphora: typical and atypical radiologic features. Neurosurg Rev 2017;40:87–94.
75. Adamek D, Malec M, Grabska N, et al. Ecchordosis physaliphora: a case report and a review of notochord-derived lesions. Neurol Neurochir Pol 2011;45:169–73.
76. Macdonald RL, Cusimano MD, Deck JH, et al. Cerebrospinal fluid fistula secondary to ecchordosis physaliphora. Neurosurgery 1990;26:515–8 [discussion: 518-519].
77. Lagman C, Varshneya K, Sarmiento JM, et al. Proposed diagnostic criteria, classification schema, and review of literature of notochord-derived ecchordosis physaliphora. Cureus 2016. https://doi.org/10.7759/cureus.547.
78. Takeyama J, Hayashi T, Shirane R. Notochordal remnant-derived mass: ecchordosis physaliphora or chordoma? Pathology (Phila) 2006;38:599–600.
79. Derakhshani A, Livingston S, William C, et al. Spontaneous, intrasphenoidal rupture of ecchordosis physaliphora with pneumocephalus captured during serial imaging and clinical follow-up: pathoanatomic features and management. World Neurosurg 2020;141:85–90.
80. Ng S-H, Ko S-F, Wan Y-L, et al. Cervical ecchordosis physaliphora: CT and MR features. Br J Radiol 1998;71(843):329–31. [Epub ahead of print].
81. Ghimire P, Shapey J, Bodi I, et al. Spontaneous tension pneumocephalus and pneumoventricle in ecchordosis physaliphora: case report of a rare presentation and review of the literature. Br J Neurosurg 2020;34:537–42.
82. Sun R, Ajam Y, Campbell G, et al. A rare case of ecchordosis physaliphora presenting with headache, abducens nerve palsy, and intracranial hypertension. Cureus 2020. https://doi.org/10.7759/cureus.8843.
83. Toda H, Kondo A, Iwasaki K. Neuroradiological characteristics of ecchordosis physaliphora: case report and review of the literature. J Neurosurg 1998;89:830–4.
84. Georgalas C, Terzakis D, Tsikna M, et al. Ecchordosis physaliphora: a cautionary tale. J Laryngol Otol 2020;134:46–51.
85. Kurokawa H, Miura S, Goto T. Ecchordosis physaliphora arising from the cervical vertebra, the CT and MRI appearance. Neuroradiology 1988;30:81–3.
86. Alkan O, Yildirim T, Kizilkiliç O, et al. A case of ecchordosis physaliphora presenting with an intratumoral hemorrhage. Turk Neurosurg 2009;19:293–6.
87. Appel JG, Bergsneider M, Vinters H, et al. Acromegaly due to an ectopic pituitary adenoma in the clivus: case report and review of literature. Pituitary 2012;15:53–6.
88. Wong K, Raisanen J, Taylor SL, et al. Pituitary adenoma as an unsuspected clival tumor. Am J Surg Pathol 1995;19:900–3.
89. Sarkar S, Chacko AG, Chacko G. Clinicopathological correlates of extrasellar growth patterns in pituitary adenomas. J Clin Neurosci 2015;22:1173–7.
90. Hagiwara A, Inoue Y, Wakasa K, et al. Comparison of growth hormone–producing and non–growth hormone–producing pituitary adenomas: imaging characteristics and pathologic correlation. Radiology 2003;228:533–8.
91. Zada G, Lin N, Laws ER. Patterns of extrasellar extension in growth hormone–secreting and nonfunctional pituitary macroadenomas. Neurosurg Focus 2010;29:E4.
92. Edal AL, Skjödt K, Nepper-Rasmussen HJ. SIPAP–a new MR classification for pituitary adenomas. Suprasellar, infrasellar, parasellar, anterior and posterior. Acta Radiol 1997;38:30–6.
93. Gao A, Bai J, Cheng J, et al. Differentiating skull base chordomas and invasive pituitary adenomas with conventional MRI. Acta Radiol 2018;59:1358–64.
94. Kuo AH, Nuñez DB. Giant pituitary adenoma with inferior petrosal sinus, jugular foramen, and hypoglossal canal extension. JAMA Otolaryngol Neck Surg 2020;146:82.
95. Riccio L, Donofrio CA, Tomacelli G, et al. Ectopic GH-secreting pituitary adenoma of the clivus: systematic literature review of a challenging tumour. Pituitary 2020;23:457–66.
96. Mudd PA, Hohensee S, Lillehei KO, et al. Ectopic pituitary adenoma of the clivus presenting with apoplexy: case report and review of the literature. Clin Neuropathol 2012;31:24–30.
97. Abele TA, Yetkin ZF, Raisanen JM, et al. Non-pituitary origin sellar tumours mimicking pituitary macroadenomas. Clin Radiol 2012;67:821–7.
98. Donovan JL, Nesbit GM. Distinction of masses involving the sella and suprasellar space:

specificity of imaging features. Am J Roentgenol 1996;167:597–603.
99. Anand P, Chwalisz BK. Inflammatory disorders of the skull base: a review. Curr Neurol Neurosci Rep 2019;19:96.
100. Khan M, Quadri SQ, Kazmi A, et al. A comprehensive review of skull base osteomyelitis: diagnostic and therapeutic challenges among various presentations. Asian J Neurosurg 2018;13:959.
101. Álvarez Jáñez F, Barriga LQ, Iñigo TR, et al. Diagnosis of skull base osteomyelitis. RadioGraphics 2021;41:156–74.
102. Jain N, Jasper A, Vanjare HA, et al. The role of imaging in skull base osteomyelitis: reviewed. Clin Imaging 2020;67:62–7.
103. Sokołowski J, Lachowska M, Karchier E, et al. Skull base osteomyelitis: factors implicating clinical outcome. Acta Neurol Belg 2019;119:431–7.
104. Ozgen B, Oguz KK, Cila A. Diffusion MR imaging features of skull base osteomyelitis compared with skull base malignancy. Am J Neuroradiol 2011;32:179–84.
105. Ryu G, Cho H-J, Lee KE, et al. Clinical significance of IgG4 in sinonasal and skull base inflammatory pseudotumor. Eur Arch Otorhinolaryngol 2019;276:2465–73.
106. Alyono JC, Shi Y, Berry GJ, et al. Inflammatory pseudotumors of the skull base: meta-analysis. Otol Neurotol 2015;36(8):1432–8.
107. Marinelli JP, Marvisi C, Vaglio A, et al. Manifestations of skull base IgG4-related disease: a multi-institutional study. Laryngoscope 2020;130:2574–80.
108. Cain RB, Colby TV, Balan V, et al. Perplexing lesions of the sinonasal cavity and skull base: IgG4-related and similar inflammatory diseases. Otolaryngol Neck Surg 2014;151:496–502.
109. Han MH, Chi JG, Kim MS, et al. Fibrosing inflammatory pseudotumors involving the skull base: MR and CT manifestations with histopathologic comparison. AJNR Am J Neuroradiol 1996;17(3):515–21. [Epub ahead of print].
110. Desai SV, Spinazzi EF, Fang CH, et al. Sinonasal and ventral skull base Inflammatory pseudotumor: a systematic review: skull base inflammatory pseudotumor. Laryngoscope 2015;125:813–21.
111. Kiessling PT, Marinelli JP, Peters PA, et al. Cranial base manifestations of granulomatosis with polyangiitis. Otolaryngol Neck Surg 2020;162:666–73.
112. Keni SP, Wiley EL, Dutra JC, et al. Skull base Wegener's granulomatosis resulting in multiple cranial neuropathies. Am J Otolaryngol 2005;26:146–9.
113. Sharma A, Deshmukh S, Shaikh A, et al. Wegener's granulomatosis mimicking skull base osteomyelitis. J Laryngol Otol 2012;126:203–6.
114. Todd Andrews J, Kountakis SE. Wegener's granulomatosis of the skull base. Am J Otolaryngol 1996;17:349–52.
115. Moore KR, Fischbein NJ, Harnsberger HR, et al. Petrous apex cephaloceles. AJNR Am J Neuroradiol 2001;22(10):1867–71. [Epub ahead of print].
116. Connor SEJ, Leung R, Natas S. Imaging of the petrous apex: a pictorial review. Br J Radiol 2008;81:427–35.
117. Jamjoom DZ, Alorainy IA. The association between petrous apex cephalocele and empty sella. Surg Radiol Anat 2015;37:1179–82.
118. Schmalfuss IM, Camp M. Skull base: pseudolesion or true lesion? Eur Radiol 2008;18:1232–43.
119. Moore KR, Harnsberger HR, Shelton C, et al. Leave me alone lesions of the petrous apex. AJNR Am J Neuroradiol 1998;19(4):733–8. [Epub ahead of print].
120. Roland PS, Meyerhoff WL, Judge LO, et al. Asymmetric pneumatization of the petrous apex. Otolaryngol Neck Surg 1990;103:80–8.
121. Arriaga MA. Petrous apex effusion: a clinical disorder. Laryngoscope 2006;116:1349–56.
122. Yildirim M, Senturk S, Guzel E, et al. Bilateral symptomatic petrous apex effusion. Indian J Otolaryngol Head Neck Surg 2010;62:186–8.
123. Chapman PR, Gaddamanugu S, Bag AK, et al. Vascular lesions of the central skull base region. Semin Ultrasound CT MRI 2013;34:459–75.
124. Moonis G, Hwang CJ, Ahmed T, et al. Otologic manifestations of petrous carotid aneurysms. AJNR Am J Neuroradiol 2005;26(6):1324–7. [Epub ahead of print].
125. Tamada T, Mikami T, Akiyama Y, et al. Giant petrous internal carotid aneurysm causing epistaxis: a case report. J Clin Neurosci 2018;58:221–3.
126. Borha A, Patron V, Huet H, et al. Endovascular management of a giant petrous internal carotid artery aneurysm in a child. Case report and literature review. Childs Nerv Syst 2019;35:183–6.
127. Liu JK, Gottfried ON, Amini A, et al. Aneurysms of the petrous internal carotid artery: anatomy, origins, and treatment. Neurosurg Focus 2004;17:1–9.
128. Murai Y, Shirokane K, Kitamura T, et al. Petrous internal carotid artery aneurysm: a systematic review. J Nippon Med Sch 2020;87:172–83.
129. Kim S-M, Kim C-H, Lee C-Y. Petrous carotid aneurysm causing pulsatile tinnitus: case report and review of the literature. J Cerebrovasc Endovasc Neurosurg 2018;20:35–9.
130. Cano-Duran AJ, Sanchez Reyes JM, Corbalan Sevilla MT, et al. Carotid petrous segment aneurysm presenting as hypoglossal nerve palsy. Neuroradiology 2021;63:447–50.
131. Hamamoto Filho PT, Machado VC, Macedo-de-Freitas CC. A giant aneurysm from the petrous carotid presenting with isolated peripheral facial palsy. Rev Assoc Médica Bras 2013;59:531–3.